Revealing the critical role of radical-involved pathways in high temperature cyclopentanone pyrolysis

Revealing the Critical Role of Radical-involved Pathways in High Temperature Cyclopentanone Pyrolysis

Xiaorui Dong[a], Erik Ninnemann[b], Duminda S. Ranasinghe[a], Andrew Laich[b], Robert Greene[b], Subith S. Vasu[b], William H. Green[a*]

[a] *Department of Chemical Engineering, Massachusetts Institute of Technology, Cambridge, MA 02139, USA*
[b] *Center for Advanced Turbomachinery and Energy Research (CATER), Mechanical and Aerospace Engineering, University of Central Florida, Orlando, FL 32816, USA*

* Corresponding author. *Email address*: whgreen@mit.edu (W. H. Green).

Abstract

Cyclopentanone (CPO) is a promising biofuel for spark-ignition engines due to its ring strain and high auto-ignition resistance. Understanding CPO decomposition is crucial for building a high-temperature combustion model. Here we present a comprehensive kinetic model for high-temperature pyrolysis of CPO with verified results from high-pressure shock tube (HPST) measurements. The time- histories of carbon monoxide (CO), ethylene (C_2H_4), and CPO absorbances over the temperature range of 1156-1416 K and pressure range of 8.53-10.06 atm were measured during current experiments. A corresponding detailed kinetic model was generated using the Reaction Mechanism Generator (RMG) with dominant unimolecular/radical-involved decomposition pathways from either previous studies or quantum calculations within the current work. The obtained model containing 821 species and 79,859 reactions exhibited a good agreement with the experimental results. In this study, the absorbance ratio between C_2H_4 and CO was used as an important factor to validate models and to prove that radical-involved bimolecular pathways were as significant as unimolecular decomposition of CPO. The rate of production (ROP) analysis showed H radicals play a major role in the decomposition, and the whole decomposition process could be divided into three stages based on the H radical concentration. The insights from present work can be used to generate a better CPO combustion model and help evaluate CPO as an advanced biofuel.

Keywords: cyclopentanone, pyrolysis, reaction mechanism

1 Introduction

In recent years, biofuels have been receiving much attention from both academia and industry, as they can be used as alternatives or additives to fossil fuels to reduce greenhouse emissions and improve the performance of blend fuels. Cyclopentanone (CPO) is one of the promising biofuel candidates identified by the U.S. Department of Energy (DOE) for advanced engines [1]. From the production side, CPO can be efficiently produced from a fungus-involved cellulose breakdown process and also from the pyrolysis of biomass [2]. From the implementation side, CPO has a relatively high energy density due to its ring strain (ring strain energy equals to 41 kJ/mol [3]), and also a high auto-ignition resistance, as shown in Table 1, making it applicable in aviation fuels and as a performance booster in spark-ignition internal combustion engines. Because of its potential, several theoretical models of combustion and pyrolysis of CPO have been built, and related experiments have been conducted to provide insights to related kinetics and to prove the feasibility of CPO as a commercial biofuel.

As usual, radical-involved oxidation pathways are the main pathways occurring in the combustion of CPO. However, previous kinetic studies mentioned that CPO decomposition dominates at high temperatures [4,5]. The same classes of decomposition reactions occur in both combustion and pyrolysis processes. Thus, establishing a better understanding of the pyrolysis process of CPO is crucial in building a more reasonable

model for its combustion and making an accurate prediction of several critical performance properties, such as ignition delay.

Table 1. Octane numbers and sensitivities of several promising biofuels and conventional blendstock [6]

Fuels	RON	MON	Sensitivity*
cyclopentanone	**101**	**89**	**12**
methanol	109	89	20
ethanol	109	90	19
n-propanol	104	89	15
isobutanol	105	90	15
prenol	93	74	19
di-isobutylene	106	87	19
2-methylfuran	103	86	17
E10 premium	98	90	8
CBOB	94	87	6
CARBOB	85	81	4

E10: Petroleum-derived gasoline containing 10 vol% ethanol; CBOB: Conventional blendstock for oxygenate blending; CARBOB: California reformulated blendstock for oxygenate blending.
* Some values for S may appear different than RON – MON based on values in table due to rounding.

The earliest studies about CPO pyrolysis date back to the middle of the 20th century [7,8]. Johnson and Walters [7] used cylindrical Pyrex reaction vessels to conduct thermal decomposition of cyclopentanone at 761-816 K and 0.130-0.413 atm. Based on infrared absorption spectroscopy as well as measurements of several physical properties, multiple chemical species were identified as products or intermediates of the process, including CO, ethylene, 1-butene, H_2 and 2-cyclopenten-1-one. The influence of temperature, pressure, and concentration of unsaturated hydrocarbons on the product distribution and the decomposition rate were investigated. They found that the process was autocatalytic, as butene and propylene exhibited accelerating effects. Later, Delles et al. conducted a similar study at 806-854 K and 0.014-0.039 atm with more advanced infrared spectroscopy, mass spectrometry, and gas chromatography as product identification methods [8]. Their results generally agreed with Johnson and Walter's findings of the decomposition reactions and the generation rate of products. Moreover, Delles et al. confirmed that the decomposition was autocatalytic and indicated that a portion of the decomposition underwent a free radical process. However, these early studies only covered a narrow range of conditions and were not specific to engine design or fuel evaluation purposes. Furthermore, the analytical methods used were not as advanced as methods available today. Thus new insights, especially further quantitative thermodynamic/kinetic details and more comprehensive analysis of the involved reactions and species, are needed for proper evaluation of CPO's potential as a fuel.

During the past five years, several studies of CPO pyrolysis were performed, wherein theoretical studies were emphasized, and experimental works were usually regarded as validations for the theoretical work [9–13]. Zaras et al. [9] identified several primary unimolecular decomposition pathways of cyclopentanone pyrolysis. They used the G3B3 quantum chemistry method [14], a modified version of the G3 method [15], to calculate the wells and transition states. The RRKM method was used to obtain reaction rate coefficients

at 800-2000 K. Based on Zaras et al.'s calculations, three main pathways were identified: (1) concerted, (2) stepwise decomposition to 2 C_2H_4 + CO, and (3) keto-enol tautomerism (Fig. 1).
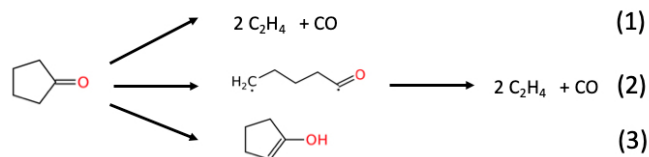

Figure 1. Main unimolecular decomposition pathways of CPO identified by Zaras et al. [9].

Within the temperature range of this study, these three pathways were orders of magnitude faster than other unimolecular pathways. Zhou et al. [10] further calculated several radical-involved decomposition pathways, including H abstraction reactions by H and CH_3 radicals at α or β sites. These decomposition pathways were a complement to the result of Zaras et al. Pastoors et al. [11] used mass-selected threshold photoelectron spectroscopy (ms-TPES) to identify major products from thermal decomposition of cyclopentanone between 800-1100 K and proposed several possible decomposition pathways which was consistent with Zaras's and Zhou's results. Pastoors et al. also mentioned that enol acted as a short-lived intermediate and appeared to play a crucial role in the thermal CPO decomposition potential energy surface (PES).

In our recent publication, we reported shock tube experiments on CPO pyrolysis at 1173-1416 K and 8.97 -9.69 atm to validate the theoretical understanding [12] and compared our results with two reported detailed kinetic mechanisms: the Zhang et al. [4] model developed at the Lawrence Livermore National Laboratory (LLNL) and Thion et al. [5] model developed at the Institute for Engineering and Systems Sciences (INSIS). Both models selectively introduced parameters from Zaras et al. and Zhou et al. Although these two models were built specifically for combustion, they possessed reasonable consistency with experimental results due to the inclusion of non-oxygen-involved pathways. The comparison of CO mole fraction time-histories, shown in Fig 2, revealed that at relatively high temperature (>1300K), Thion's mechanism was in a good agreement with experiments, while the LLNL mechanism underestimated the rate and the yield of CO. At lower temperature (<1200K), both mechanisms underestimated the rates.
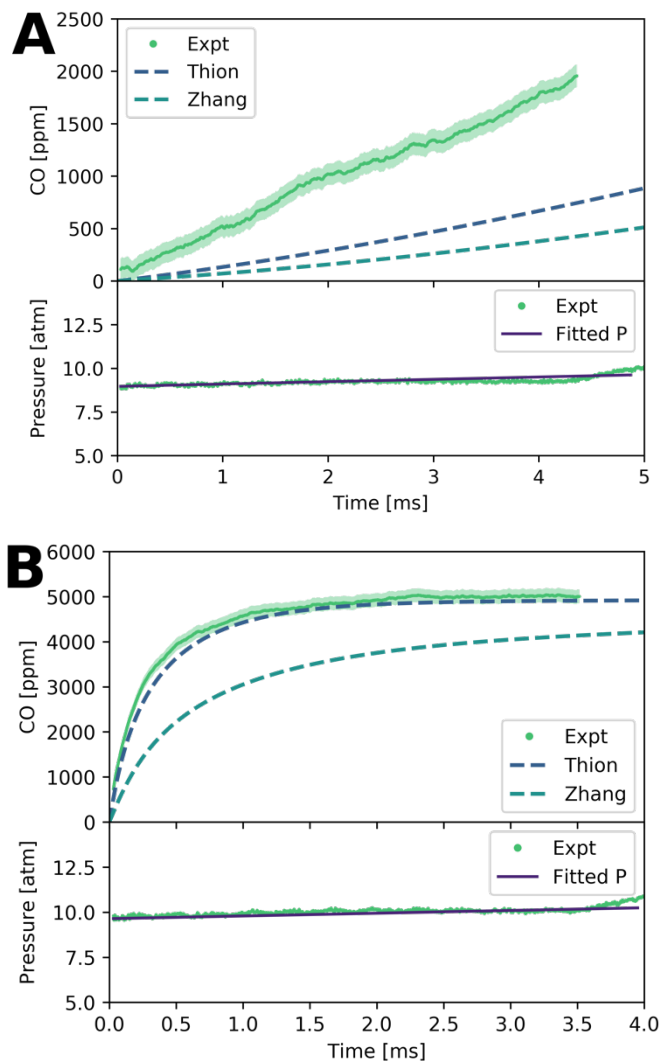
Figure 2. Time-histories of the CO mole fraction and pressure under different conditions modified from [12]. (A) $T_5 = 1173K$, $P_5 = 8.97$ atm, $x_{CPO,0} = 0.5\%$ and $x_{Ar,0} = 99.5\%$. (B) $T_5 = 1367$ K, $P_5 = 9.69$ atm, $x_{CPO,0} = 0.5\%$ and $x_{Ar,0} = 99.5\%$. In the mole fraction subgraph, the green dotted line is the experimental CO time-history with its uncertainty indicated, the purple dashed line is the prediction according to Thion's model, and the green dotted line is the prediction from Zhang's model. In the pressure subgraph, the green dotted line is the experimental pressure time-history, while the purple solid line is the fitted pressure time-history used as boundary condition in the ideal gas adiabatic simulation.

To resolve the discrepancy between the theoretical models and the experiments, Giri et al. [13] proposed a fitting strategy where the energy barrier for the concerted decomposition pathway (Eq. (1)) was reduced by 1.5 kcal/mol. Moreover, they performed master equation simulations using MultiWell [16–18] and showed such modification would yield over 95% CPO outflux proceeding via pathway (1). The total decomposition rate from their simulation was consistent with the experimental (from shock tube) above 1250 K, while a slight discrepancy still could be seen at 1150 K.

Rather than empirically fitting a mechanism to match the experimental results, we hypothesize that the discrepancy is caused by missing or underestimating certain decomposition pathways. This hypothesis is supported by the experimental study by Delles et al. [8], but for better verfication, the information on the

branching ratio needs to be obtained. The branching ratio can be determined from the concentrations of radical intermediates. However, experimentally measuring these concencentrations is often challenging. Instead, in this publication, we demonstrate an effective strategy to validate the hypothesis combining experiments and kinetic modeling. Further, we reveal the importance of radical-involved pathways in CPO decomposition with our validated mechanism and provide a comprehensive picture for CPO pyrolysis.

2 Experiments

2.1 Shock tube setup

To validate the model, carbon monoxide (CO), ethylene (C_2H_4), and cyclopentanone (CPO) absorbance time-histories were collected in a double-diaphragm, heated, high-pressure shock tube facility at the University of Central Florida (UCF) with an internal diameter of 0.1417 m. Specific details of the shock tube facility can be found in [19–21]. The velocity of the incident shock wave was measured through five piezoelectric pressure transducers (wired to four time-interval counters). The temperature (T_5) and pressure (P_5) behind the reflected shock were calculated through quasi one-dimensional normal shock relations using the measured incident shock velocity. The calculated uncertainty of T_5 and P_5 was around 10 K ($\pm$0.8%) and 0.14 atm ($\pm$1.5%), respectively. Eight equally spaced ports around the circumference of the tube, 2.00 cm away from the end-wall, were used for pressure and spectroscopic measurements. Time-zero for each experiment was set to the minimum of the schlieren spike on the laser trace measurement. To prevent condensation of CPO, fuel mixtures composed of CPO (with a concentration range of 770-8000 ppm) and argon were made at a facility temperature of 80 ºC, whose fuel partial pressure was well below the vapor pressure of CPO according to a fit equation from Kobe et al. [22] and Barhala et al. [23].

2.2 CO absorbance time-histories

Carbon monoxide absorbances were measured using a continuous wave, distributed feedback quantum cascade laser (DFB QCL) centered at 2046.30 cm^{-1} from Alpes Lasers (TO3-L-50) without interference from other species (Supplementary information Fig. S1.2(D)). To ensure the spectral output from the laser remained stable during shock tube experiments, the laser was monitored via a Bristol 771 Spectrum Analyzer throughout each test. The schematic of the laser setup is shown in Fig. 3.
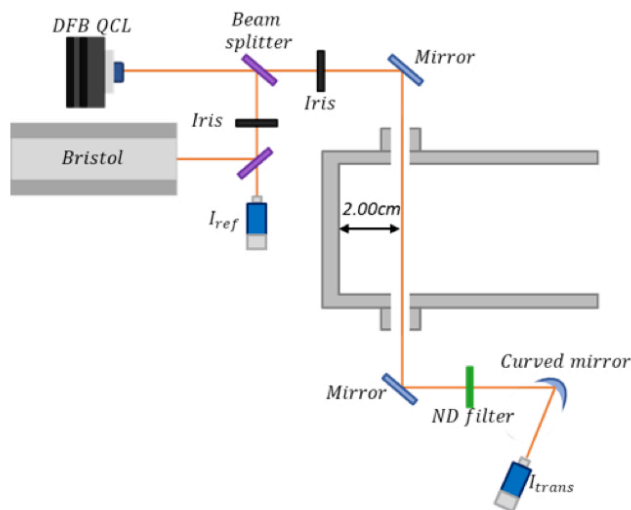

Figure 3. Schematic of shock tube and laser setup used to measure CO time-histories.

To compare with the experimental absorbances, we used the Beer-Lambert Law, Eq. (4), to convert the modeled mole fraction values into absorbances:

$$\alpha = \frac{\sigma P L}{RT} X \qquad (4)$$

where α is the absorbance, P is the total pressure of the gas mixture (Pa), T is the temperature of the mixture (K), L is the path length of the absorbing species (m), R is the universal gas constant (J/mol/K), and σ is the absorption cross-section of the absorbing species (m^2/mol). The absorption cross-section of CO was measured behind reflected shockwaves in the UCF shock tube to characterize its dependence on thermodynamic parameters between 1085-1456 K and pressures of 8.6-10.3 atm. A mixture composition of 1% CO/ 12% He/ 86% Ar was used for these cross-section measurements; the addition of helium decreases the relaxation time of CO ensuring the measurements are made on ground state species. A power law fit in both temperature (K) and pressure (Pa), Eq. (5) yields great agreement with experimentally obtained cross-sections (m^2/mol) when $A = 9.1120 \times 10^6$ m^2/mol, $B = -1.1320$, and $C = 0.3160$:

$$\sigma = A P^B T^C \qquad (5)$$

2.3 CPO absorbance time-histories

For CPO quantification, two different lasers were used in two separate experimental campaigns. In the first measurement campaign, a DFB ICL from Nanoplus was tuned to 2929.50cm^{-1} and 2938.25cm^{-1} in an attempt to measure CH_4 with a two-color subtraction scheme to rid the measurement of interfering species; although, this scheme was not fruitful due to initial concentration variance. Despite the partial pressure of CPO in the mixture being held below its saturation vapor pressure at the experimental temperature (saturation vapor pressure of CPO > 30 Torr if temperature > 50 °C [23]), we observed inconsistencies in the initial CPO concentrations in the shock tube, suggesting some CPO had been lost from the gas phase. In order to quantify the initial CPO concentration, FTIR measurements (provided in supplementary Figure S1.3B) were utilized, and the starting concentration was found to vary from its nominal value by 60%, with a max uncertainty in the measured concentration of 11.5%. Possible reasons for the concentration variance could be the fuel condensing inside the tube test section as the fuel is expanded from the fill line into the large volume of the tube or fuel adhesion inside the fuel line. Nonetheless, the starting concentration for each experiment was quantified, and this value was used for all subsequent calculations. In these measurements, other hydrocarbon intermediates and products could interfere with CPO quantification in the intermediate and late stages of the reaction. Therefore for some figures displayed, CPO time-histories and C_2H_4 time-histories are truncated to remove the data strongly perturbed by the interference (due to the dependence of CPO on C_2H_4 discussed in the next section). We used the current mechanism to estimate the interference of the CPO and C_2H_4 measurement. The CPO trace is truncated at 90% of the time when C_2H_4 absorbance contributed 2% to the total absorbance. Likewise, the C_2H_4 traces were not shown until 110% of the simulated time when CPO was fully depleted.

Due to the interference in the first campaign, the measuring strategy was adjusted in the second. In the second campaign, we used a DFB QCL centered at 1749.84cm^{-1} from MIRSense for interference-free CPO quantification (Supplementary information Fig. S1.2(C)). To mitigate concentration variance in this campaign, the CPO concentration in the mixture was reduced from 0.25% to 0.10%, and the tube and the mixing tank were maintained at 80°C. While these precautions helped, they did not fully alleviate the

changes in starting fuel concentration. Therefore, for the initial CPO concentration measurement, the absorption cross-section of CPO was first measured by vaporizing the pure compound into the driven side of the tube and measuring the absorbance at 80 ℃ and different filling pressures. From the slope of the absorbance-pressure curve (Supplementary information Fig. S1.3), the CPO cross-section at the specified wavelength and temperature was measured to be 20.24 m^2/mol. Then, this same stage-filling procedure was used prior to each experiment to extract the initial concentration of CPO, using the measured cross-section. The average initial concentration uncertainty was calculated to be $\pm 8\%$. From the measured initial concentration, the absorption cross-sections of CPO for all conditions were obtained from the absorbance plot immediately behind the reflected shockwave.

2.4 C_2H_4 absorbance time-histories

Ethylene absorbance was measured with a tunable CO_2 gas laser (Access Laser L4GS) centered at 949.49 cm^{-1}. Near this wavelength, CPO also has an absorption feature (Supplementary information Fig. S1.2(A) and (B)). Therefore the contribution from CPO must be subtracted to obtain C_2H_4 time-histories, and the derived formula for C_2H_4 absorbance is

$$\alpha_{949,C_2H_4} = \alpha_{949,\text{total}} - \alpha_{\lambda_2,\text{CPO}} \frac{\sigma_{949,\text{CPO}}}{\sigma_{\lambda_2,\text{CPO}}} \tag{6}$$

$\sigma_{949,CPO}$ is the cross-section of CPO at ethylene's measured wavelength (949.49cm^{-1}), $\sigma_{\lambda_2,CPO}$ is the cross-section of CPO at the wavelength where CPO can be measured interference free ($\lambda_2 = 2938.25cm^{-1}$ or 2929.50cm^{-1} in the first experimental campaign and $\lambda_2 = 1749.84cm^{-1}$ in the second experimental campaign), $\alpha_{949,\text{total}}$ is the total measured absorbance due to all absorbing species at 949.49cm^{-1}, α_{949,C_2H_4} is the absorbance at 949.49cm^{-1} due only to C_2H_4, and $\alpha_{\lambda_2,\text{CPO}}$ is the absorbance of CPO at its separately measured wavelength. In the model validation, we still used the Beer-Lambert Law to convert C_2H_4 concentrations into C_2H_4 absorbances, and the C_2H_4 cross-section values were calculated according to the temperature and pressure correlation reported by Ren et al. [24] and verfified in our recent work [25].

3   Theoretical studies

The computational work was divided into three phases. In the first phase, quantum chemistry calculations for important species and transition states were conducted using Gaussian 03 [26] and Gaussian 16 [27]. These results were imported into Arkane, a package distributed with Reaction Mechanism Generator (RMG) [28,29], to generate thermodynamic and kinetic data. Secondly, RMG was used to generate detailed mechanisms with updated parameters. Finally, CHEMKIN-PRO [30] and Reaction Mechanism Simulator (RMS) [31] were used to simulate the pyrolysis of cyclopentanone under shock tube conditions and generate concentration time-histories and rate of production (ROP) results. Concentration data were converted to absorbances using Beer-Lambert Law to validate the model with experimental data, while ROP results were used to understand the pyrolysis process.

3.1   Quantum chemistry calculation

Single point energies (for both ground states and transition states), optimized geometries, and harmonic frequencies were calculated with the CBS-QB3 quantum chemistry method [32]. If a species contained hindered rotors, rotation scans were performed on the corresponding dihedrals with 72 steps of 5º increments (covering 360º) at the B3LYP/CBSB7 level of theory. Intrinsic reaction coordinate (IRC)

calculations were performed to make sure that the transition states were corresponding to the correct reaction paths connecting the reactants and products.

Arkane was used to calculate thermodynamic and kinetic parameters according to the Gaussian output files. The rigid rotor harmonic oscillator (RRHO) approximation with 1D hindered rotor correction as well as the conventional transition state theory was used as the theoretical foundation. Results were exported in commonly used formats (NASA polynomials for thermodynamic properties, modified Arrhenius formula for high-pressure limit rate coefficients, and Chebyshev Polynomial for pressure-dependent rate coefficients) to update RMG libraries.

The majority of calculations conducted in the current work were aimed at filling the gaps in primary reactions and species which had not been calculated in previous publications. They included calculations of CPO beta C-C homolysis reaction and H radical addition reactions. Previously, the concerted decomposition reaction (1) was identified as the most important pathway taking up most of the fluxes, so we recalculated this reaction at CCSD(T)-F12/cc-pVZ-f12 extrapolation to the complete basis set (CBS) [33] limit with geometries and frequencies calculated at APFD/6-311+G(2d,p) level of theory [34] using Gaussian 16 [27] and Molpro [35,36]. The new calculation showed that the barrier was 339.0 kJ/mol, and the high-pressure-limit rate coefficient curve reached a good agreement with calculations from Zaras et al. (Fig. 4). Cartesian coordinates of ground and transition state structures and rate coefficient parameters of reactions are provided in the supplementary information section S2.
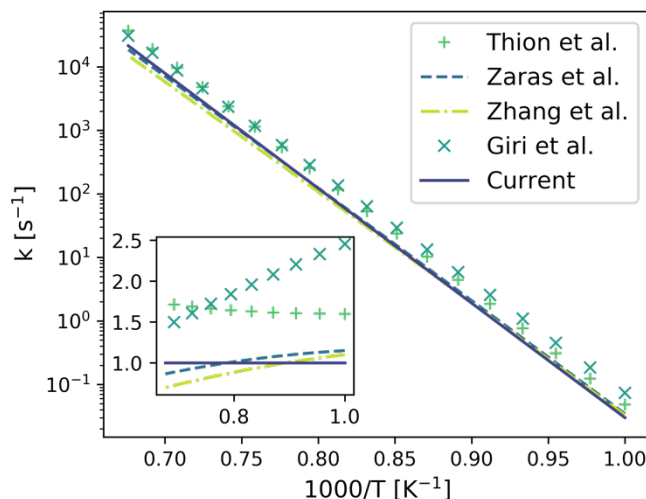

Figure 4. High-pressure-limit rate coefficients of reaction (1) from different sources. The inset shows the rate coefficient values at different temperatures relative to the rate coefficient calculated in the current work.

3.2 Detailed mechanism generation

The detailed mechanism of CPO pyrolysis was generated using Reaction Mechanism Generator (RMG, version 2.3.0), an open source software package, developed primarily by the Green group at MIT [28]. RMG can automatically construct a chemical reaction mechanism depending on the flux of species. The reported mechanism, provided in the supplementary information, was built for a system with an initial mixture of 99.5% Ar and 0.5 % CPO reacting in the RMG 'range reactor' with a temperature range of 900-1400K and a pressure range of 8.00-10.00 atm. During model generation, RMG can explore the chemical space based on reaction rules and make decisions to include species and reactions into the mechanism in a self-guided manner. Data used to make a judgement or used as the final output parameters were from two kind of sources: specified values and estimated values. For specified values, important primary reactions,

including stepwise decomposition, keto-enol tautomerism from Zaras et al., radical involved decomposition from Zhou et al., and additional reactions calculated within this study were used as seed mechanisms. Further, several thermochemical libraries ('DFT_QCI_thermo', 'thermo_DFT_CCSDTF12_BAC', 'CBS_QB3_1dHR', 'CHO', 'FFCM1(-)') and kinetic libraries ('Klippenstein_Glarborg2016') were included in the simulation. These are distributed with RMG to provide accurate and reliable parameters. For species not included in the RMG libraries, their thermodynamic parameters were estimated by RMG based on the group additivity (GA) method [37]. For rate coefficients not previously specified, RMG's rate rules were used to make an estimation. The final kinetic model had 821 species and 79,859 reactions. Sensitivity analysis of the mechanism was also conducted with the aid of RMG, which helped identify the sensitive species and reactions.

3.3 Pyrolysis behavior prediction

CHEMKIN-PRO [30] and Reaction Mechanism Simulator (RMS) [31] were used to simulate the shock tube experiments. RMS is an open-source package written in Julia supporting various kinds of 0-D chemical reaction system simulations. It yields numerically consistent results compared with CHEMKIN-PRO while being more flexible for large batches of simulations and having improved performance on flux diagrams when adapting RMG outputs. Moreover, it is able to conduct bound-to-bound uncertainty analysis on initial conditions, providing a more reliable model validation approach. The reaction system in the shock tube was approximated by a 0-D ideal gas adiabatic system for model validation. As the experimental measurements suggested a constant pressure rise, we recorded the pressure profiles during the experiments and used them as boundary conditions to simulate the behavior correctly. The simulated concentration and thermodynamic parameter time-histories as well as their uncertainties were used to derive the absorbances according to the Beer-Lambert Law (Eq. (4)). The simulated fluxes results were used to conduct rate of production (ROP) analysis and generate reaction network.

4 Results and Discussions

4.1 Model validation with absorbance time-histories

The shock tube experimental results were used to validate the CPO pyrolysis model, and the species absorbances were chosen as the validating metrics. By this approach, the influence of initial condition uncertainties on species distribution can be clearly illustrated, making the validation more robust. Moreover, the correlations among temperature, pressure and mole fractions are obtained from simulations to correctly calculate the uncertainty propagation, yielding an more accurate uncertainty analysis. Fig. 5 shows the absorbance time-histories of CO, one of the major products of CPO pyrolysis.
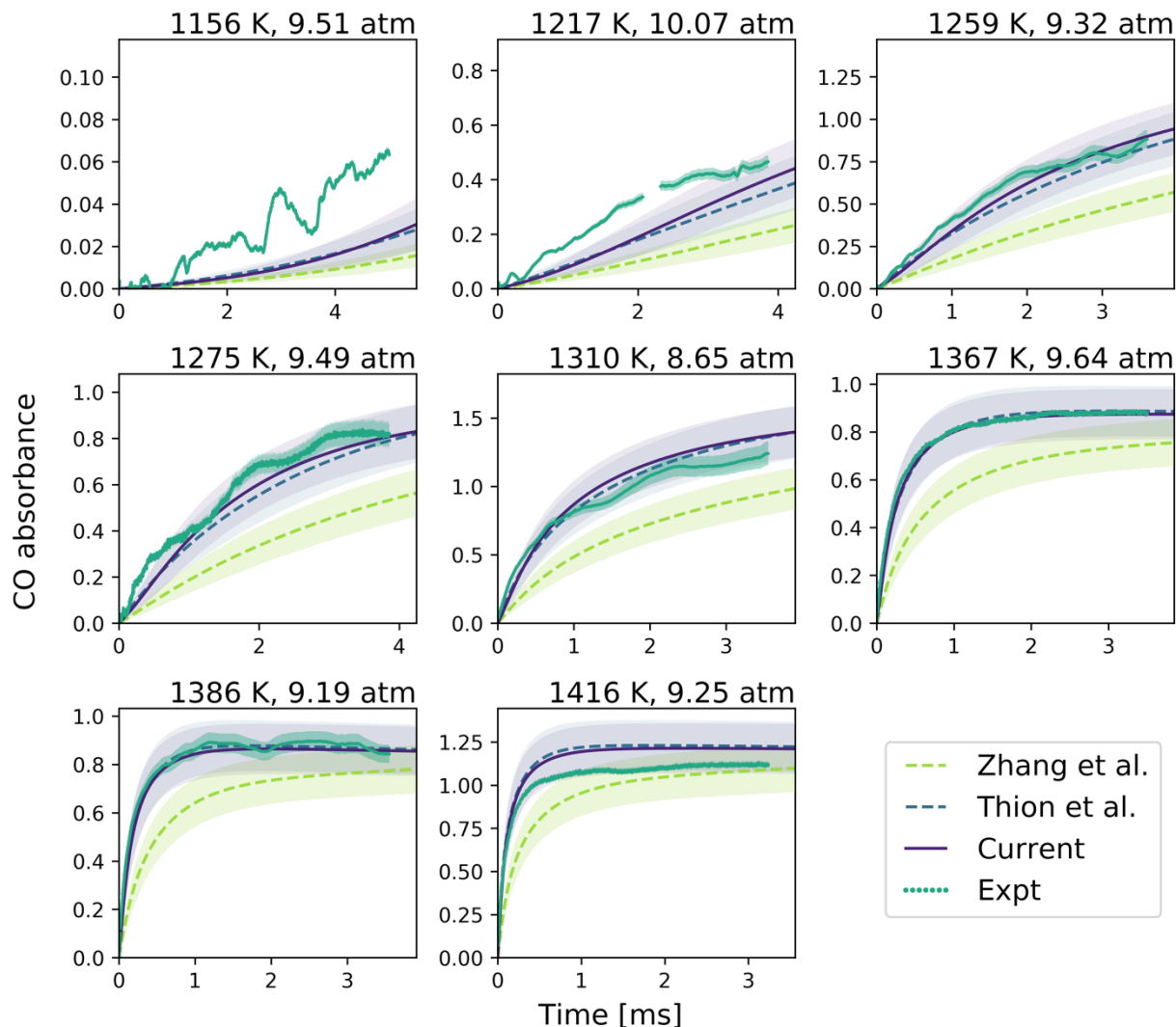
Figure 5. Time-histories of CO absorbance at different temperatures and pressures. The green dotted lines are experimental results, the purple lines are predictions from the current model, while the blue and green dashed lines are predictions from the Thion et al. and Zhang et al. models. The temperature and pressure are indicated at the top-right corner of each figure. The uncertainty of each curve is indicated by the translucent region with the same color as the curve.

Our model is in good agreement with the experimental results between 1217 and 1416 K. Further, according to the high temperature simulations where CO concentrations eventually plateaued, the predicted yields of CO (on CPO basis) are above 95%, which is consistent with the observation by Giri et al. [13]. Although comparing the CO concentration or absorbance time-histories was a common strategy in the previous studies [12,13], it can not be regarded as a decisive metric for validating a mechanism or distinguishing it from another. In CPO pyrolysis, most of the carbonyl groups from cyclopentanone eventually convert to CO, one of the most stable oxygenated species in the pyrolysis system, via either concerted/stepwise decomposition pathways (1-2) or radical-involved pathways. Although branching ratios in the current and the Thion et al. model are quite different, the CO absorbance predictions from both models overlap with each other.

More insights about the mechanisms can be unveiled by considering the time-histories of C_2H_4 absorbance, especially the absorbance ratio between C_2H_4 and CO ($\alpha_{C_2H_4}/\alpha_{CO}$). $\alpha_{C_2H_4}/\alpha_{CO}$ can be regarded as a

substitute for the mole fraction ratio between C_2H_4 and CO ($x_{C_2H_4}/x_{CO}$), which is related to the branching ratio of the system. The transformation relation is

$$\frac{\alpha_{C_2H_4}}{\alpha_{CO}} = \frac{\sigma_{C_2H_4}}{\sigma_{CO}} \frac{x_{C_2H_4}}{x_{CO}} \qquad (7)$$

Where σ_x is the absorption cross-section of the absorbing species. According to both Thion et al. and Giri et al., the concerted reaction (1) took up the most dominant flux, making most of the cyclopentanone convert to one CO molecule and two C_2H_4 molecules, yielding a $x_{C_2H_4}/x_{CO}$ ratio of approximately two. However, radical-involved decomposition pathways may be more dominant as shown in later sections. In such a scenario, CPO has a higher chance to be converted to other hydrocarbons, including butene and butadiene, which breaks the stoichiometry of the concerted reaction. Moreover, radicals also activate C_2H_4 reaction channels and let C_2H_4 be converted to other species. Thus, we expect to see a lower $x_{C_2H_4}/x_{CO}$ (and thus a lower $\alpha_{C_2H_4}/\alpha_{CO}$, according to Eq. (7)) under such a condition.

Further, from the validation point of view, we find that $\alpha_{C_2H_4}/\alpha_{CO}$ is much less sensitive to the uncertainties of initial conditions than species absorbances. We did brute force uncertainty analyses on initial conditions using the current model. The method is explained in section S4.1, and an example is shown in Fig S4.1. With the given experimental uncertainties, the relative uncertainties of the predicted $\alpha_{C_2H_4}/\alpha_{CO}$ are smaller than 4% in most cases, while the relative uncertainties of the predicted absorbances can be as large as 40% at the increasing stage and typically larger than 15% during the whole process.

Time-histories of $\alpha_{C_2H_4}/\alpha_{CO}$ as well as the CPO, C_2H_4, and CO absorbances are shown in Fig. 6, demonstrating our model is in good agreement with the experimental results, whereas the Thion et al. and Zhang et al. models show an overestimation of the $\alpha_{C_2H_4}/\alpha_{CO}$. Similar figures covering a temperature range of 1156 to 1416K are available in the supplemental material (Fig S4.2-S4.11).

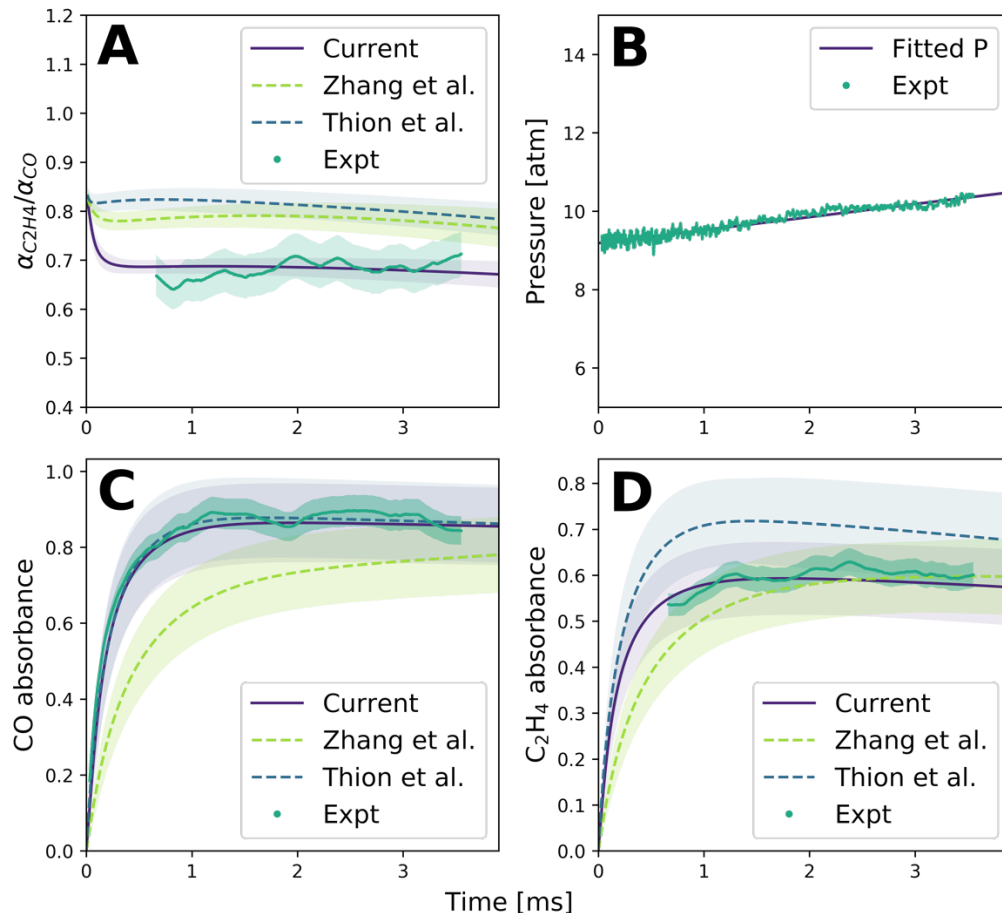**Figure 6.** HPST experiments results at $T_5 = 1393K$, $P_5 = 8.98$ atm and $x_{CPO,0} = 4000$ ppm. (A) $\alpha_{C_2H_4}/\alpha_{CO}$; (B) pressure; (C) CO absorbances; (D) C_2H_4 absorbances. For (A), (C) and (D), the purple lines are the predictions from the current model, while the blue and green dashed lines are predictions from Thion et al. and Zhang et al models., respectively, and the green dotted lines are experimental data. The uncertainty of each curve is indicated by the translucent region with the same color as the curve. For (B), the green dotted line is the measured pressure, while the purple line is the pressure fitted to the measurement used as the boundary condition for the ideal-gas adiabatic simulation.

4.2 Model correction to previous studies

To better understand the differences between the current model and former models, especially with the model of Thion et al., rate of production (ROP) analysis was performed on CO and C_2H_4 for both models (shown in Fig 7). Although the branching ratios are different, both mechanisms share similar dominant reactions. In order to check whether the differences in parameters of dominant pathways are the main causes for differences in models, we performed a recursive model correction scheme on the Thion et al. model. We either added missing pathways or replaced both thermodynamic and kinetic parameters for dominant reactions by parameters used in the current model. Once the models were corrected, we reran the simulations and compared $x_{C_2H_4}/x_{CO}$ to those from experiments or existing models. The alteration to Thion et al. model is summarized in Table 2, and the $x_{C_2H_4}/x_{CO}$ results are shown in Fig. 8. The ratio of mole fractions, rather than absorbances, is used for model-to-model comparison because reduction of experimental uncertainties is unnecessary.
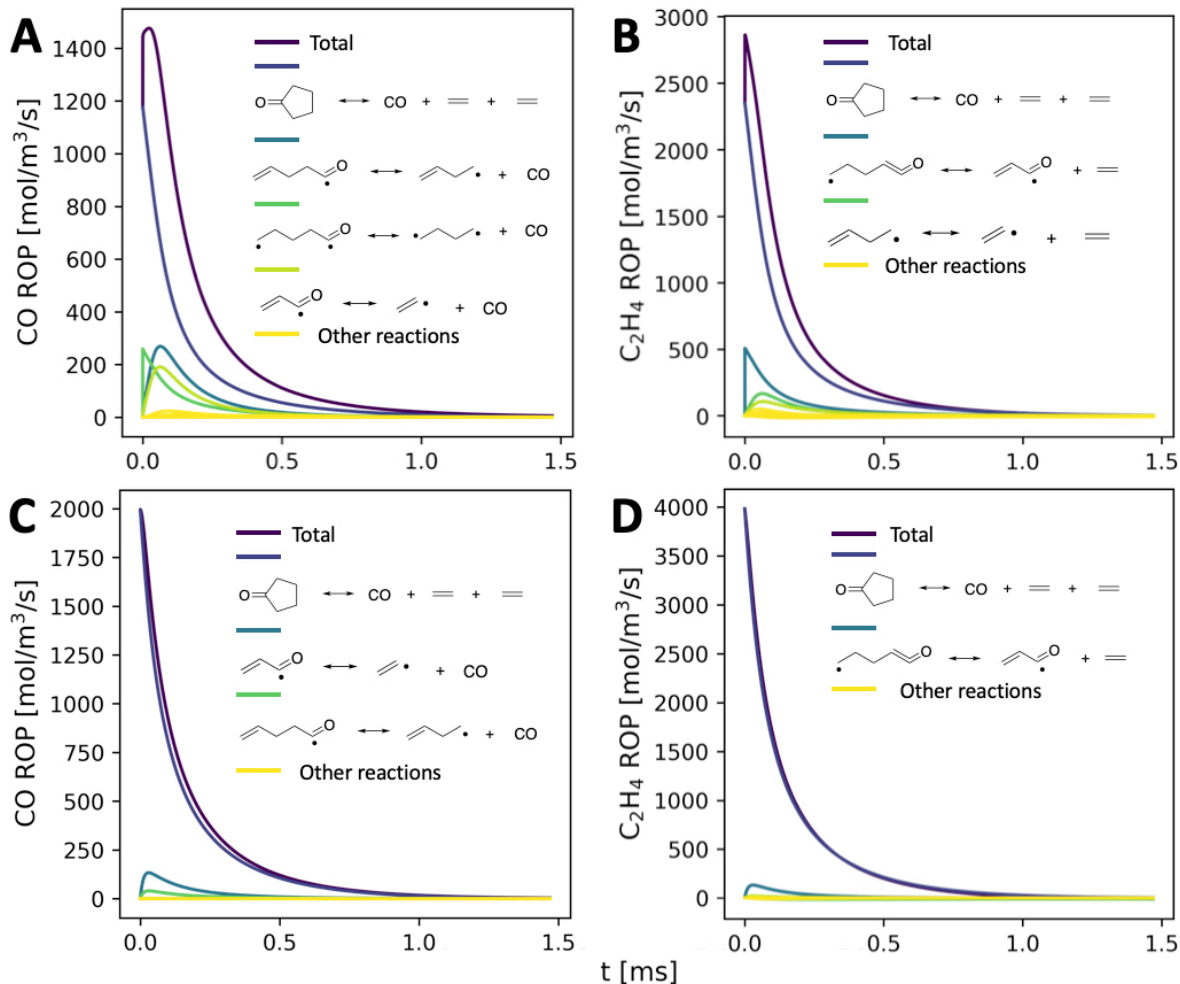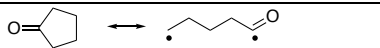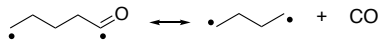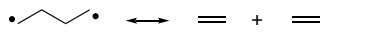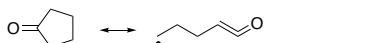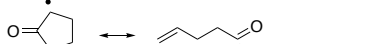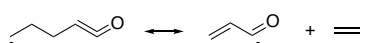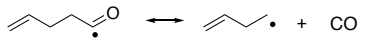
12

Figure 7. ROP analysis of C_2H_4 and CO based on the current model are shown in (A) and (B); ROP analysis based on the Thion et al. model are shown in (C) and (D). The initial condition is T_5 = 1393 K, P_5= 8.977 atm and $x_{CPO,0}$ = 4000 ppm. The reactions corresponding to each curve are indicated.

In the first round iteration, reaction pathway (2) (containing reaction (8-10)) is added, and parameters of reaction (11-14) are modified, resulting in a slight improvement to the $x_{C_2H_4}/x_{CO}$ curve ($x_{C_2H_4}/x_{CO}$ at 3.5 ms varying from 1.71 to 1.64). Then, as the concerted decomposition pathway (1) is the most dominant, we updated the model with the recalculated value (reported in the 3.1 section) in the second round correction. The update led to further improvement ($x_{C_2H_4}/x_{CO}$ at 3.5 ms varying from 1.64 to 1.57). Generally, by making corrections to important reactions, the branching ratios of the mechanisms were amended (e.g., concerted decomposition pathways are suppressed as the updated value is only half of the value being initially used as shown in Fig. 4), thus improved $x_{C_2H_4}/x_{CO}$ were obtained. However, a gap between experimental $x_{C_2H_4}/x_{CO}$ and such corrected $x_{C_2H_4}/x_{CO}$ still could be seen. Further investigation (in the 4.3 section) shows that H radical generation and recycling play essential roles in the decomposition of CPO. However, we acknowledge that the model from Thion et al. is mainly aimed to simulate high-temperature oxidative systems where such pathways are less critical.

13

Table 2. High-pressure-limit rate coefficient parameters for newly added or modified reactions to Thion's model. Ea and A are in kJ mol^{-1} and s^{-1}, respectively. Reactions (8-10) are missing in the model of Thion et al.

Reaction	#	Thion			Current		
		A	n	E_a	A	n	E_a
O=cyclopentanone ⟶ (chain)	(8)				1.5×10^{27}	-3.5	357
(chain) ⟶ (chain) + CO	(9)				1.4×10^{9}	1.1	246
(chain) ⟶ = + =	(10)				5.0×10^{12}	0.0	0.00
O=cyclopentyl ⟶ (chain)	(11)	7.3×10^{49}	-10.7	203	9.5×10^{13}	0.0	154
O=cyclopentyl ⟶ (chain)	(12)	1.1×10^{37}	-7.3	167	1.7×10^{13}	0.0	122
(chain) ⟶ (chain) + =	(13)	3.6×10^{12}	0.46	123	5.7×10^{13}	0.0	105
(chain) ⟶ (chain) + CO	(14)	2.1×10^{13}	0.32	101	6.1×10^{14}	0.0	65.3

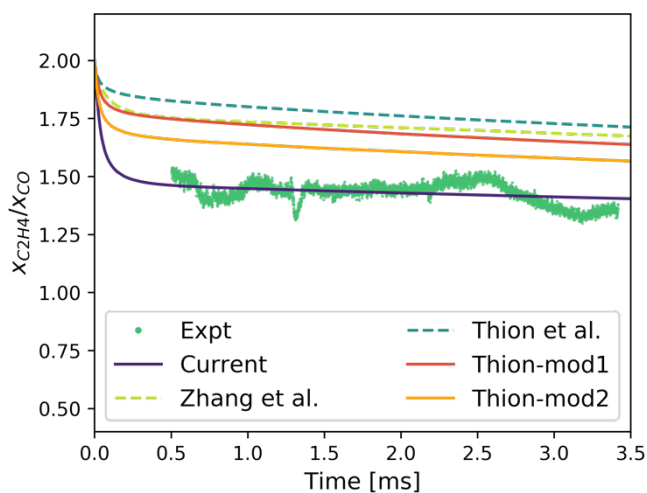**Figure 8.** $x_{C_2H_4}/x_{CO}$ time-histories from "corrected" Thion models and their comparison with other models. The initial condition is $T_5 = 1393$ K, $P_5 = 8.977$ atm and $x_{CPO,0} = 4000$ ppm. Thion-mod1 refers to the 1st stage modified Thion's mechanism, while Thion-mod2 refers to the 2nd stage modified Thion's mechanism.

4.3   The CPO pyrolysis process

To better understand the pyrolysis behavior of CPO, we calculated ROPs and sensitivities of the H radical on the current model. We found that the pyrolysis process of CPO consists of three stages associated with different H radical mole fraction (x_H) and its influence on the $x_{C_2H_4}/x_{CO}$ curve, as shown in Fig. 9.

4.3.1 Early stage

Early stage refers to a stage where significant drops can be seen in the $x_{C_2H_4}/x_{CO}$ curves (as shown in the example of Fig. 9; $x_{C_2H_4}/x_{CO}$ decreases from 2 to 1.65 in about 0.1 ms). It corresponds to the period from time-zero to the time when x_H reaches its local maximum. The length of the period is determined by the concentration and the generation rate of radicals, especially the H radical. From Figs. 9 and 10, it is clear that the increase in the concentrations of H and other radicals (including methyl and vinyl radicals) causes the branching ratio of primary CPO decomposition to change significantly. This change makes radical-involved bimolecular reactions comparable to the unimolecular pathway (1-3), which further decreases $x_{C_2H_4}/x_{CO}$. In more detail, when the concerted (1) and stepwise (2) unimolecular decomposition are the most dominant pathways ($\approx 90\%$), $x_{C_2H_4}/x_{CO}$ is close to two according to the stoichiometry. However, when H radicals (and other radicals) are involved in the reactions, we can see much more diversity in the decomposition pathways (Fig. 11). During the early stage, most of the radicals are consumed to generate $\alpha - CPO$ (2-oxo-cyclopentyl) and $\beta - CPO$ (3-oxo-cyclopentyl) radicals, which further undergo the ring-open beta-scission reactions and yield four major chain oxo-hydrocarbon radicals. While some of the intermediates can still undergo pathways with $x_{C_2H_4}/x_{CO}= 2:1$, others may yield radicals like vinyl, allyl or butenyl which eventually become acetylene, propene, butene, or butadiene, resulting in a smaller $x_{C_2H_4}/x_{CO}$. More importantly, H radicals, first consumed by CPO, will be regenerated from intermediates, catalyzing CPO decomposition via the pathways with lower barriers (as low as 14 kcal/mol [10]). However, these pathways cannot boost x_H, and other pathways are accounting for the accumulation of the radicals. According to Fig. 12 where ROP results and sensitivity analysis results are compared, pathways including the homolysis of the C-H of cyclopentanone are identified as possible H (or other radical) generation pathways, as they have a great impact on increasing the concentration of H while not participating in the catalysis cycle.
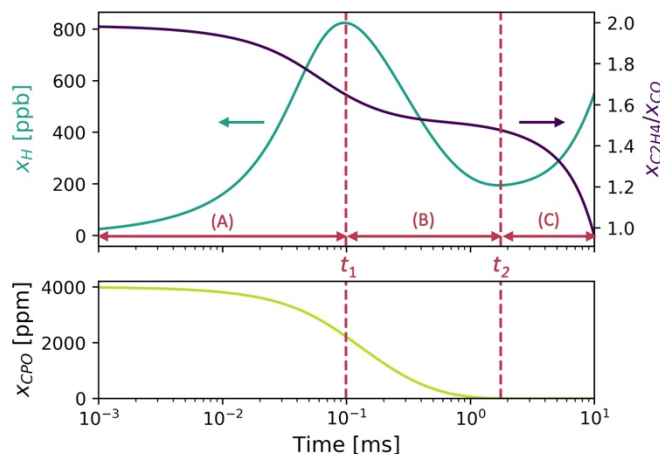

Figure 9. Stage division diagram at condition $T_5 = 1393$ K, $P_5= 8.977$ atm and $x_{CPO,0} = 4000$ ppm. Only times between 10^{-3} ms to 10 ms are shown for clarity. The upper figure shows x_H (left axis) and $x_{C_2H_4}/x_{CO}$ (right). The bottom figure shows x_{CPO}. The process is divided into three stages: (A) early stage (B) transition stage and (C) product pyrolysis. The transition between (A) and (B) occurs at 10^{-1} ms and the transition between (B) and (C) occurs at 1.76 ms for the current example.
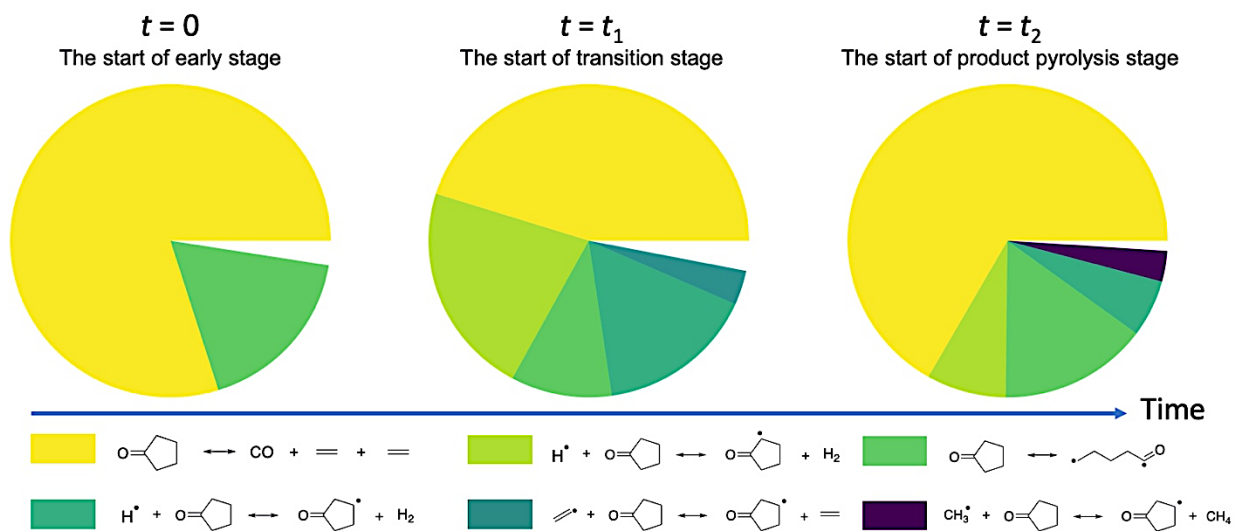
Figure 10. The instantaneous branching ratio of the primary reactions (decomposition of CPO) under the condition of T_5 = 1393 K, P_5 = 8.977 atm and $x_{CPO,0}$ = 4000 ppm at different times. At each time, the full area of the pie indicates the total outflux from CPO, and the area of each section is proportional to the ratio of the reaction flux over the total outflux. The gap in each figure is contributions from other minor reactions.
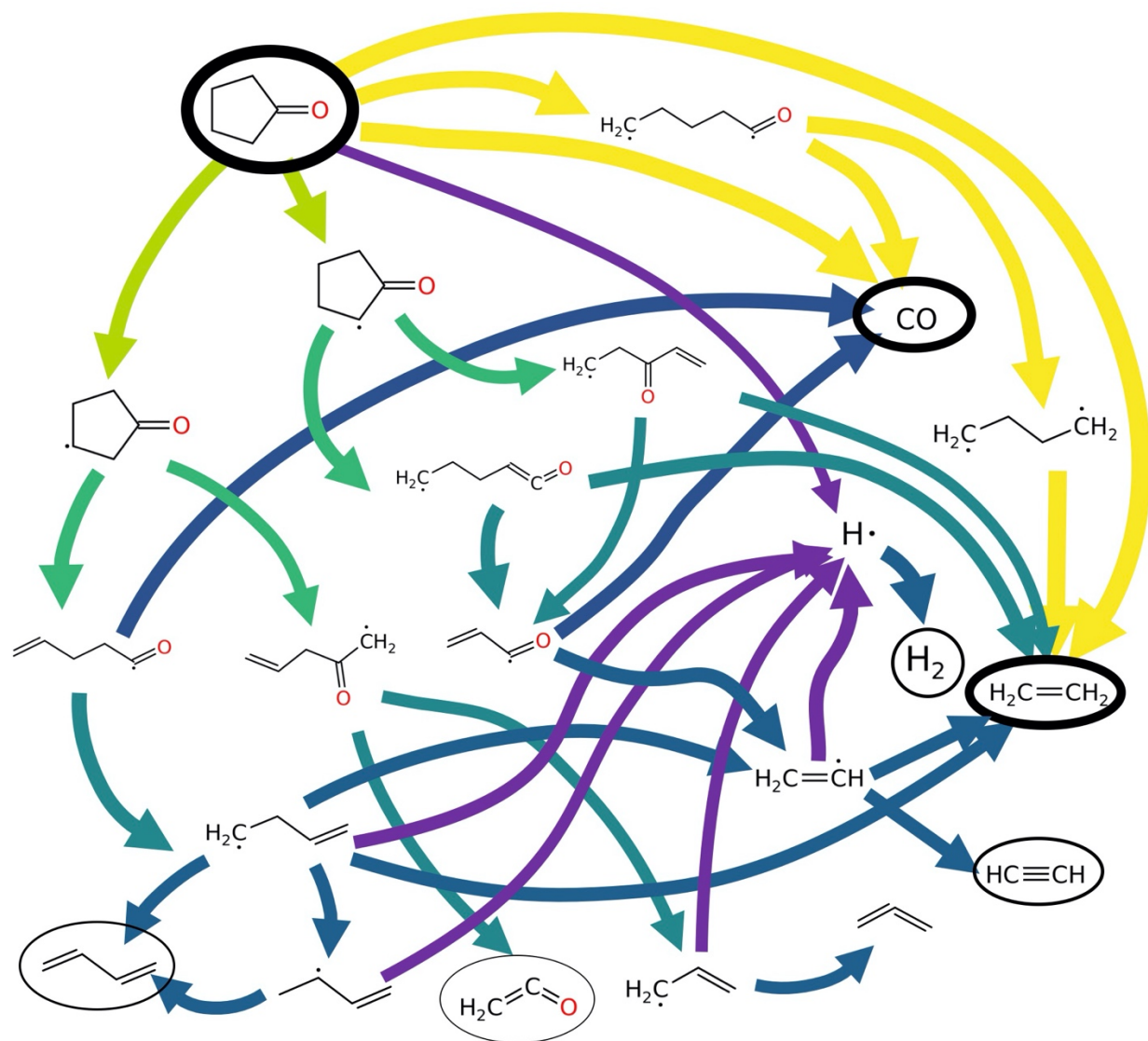
Figure 11. Dominant reaction fluxes of cyclopentanone decomposition at 0.05ms (early stage) with the condition of $T_5 = 1393$ K, $P_5 = 8.977$ atm and $x_{CPO,0} = 4000$ ppm. The boldness of the arrows indicates the relative size of the fluxes in log scale and the boldness of the circle around the species indicates the relative concentrations in log scale. The unimolecular pathways are indicated by yellow, while radical-involved pathways are indicated by other colors, and color differences are used to indicate the hierarchy of the mechanism.
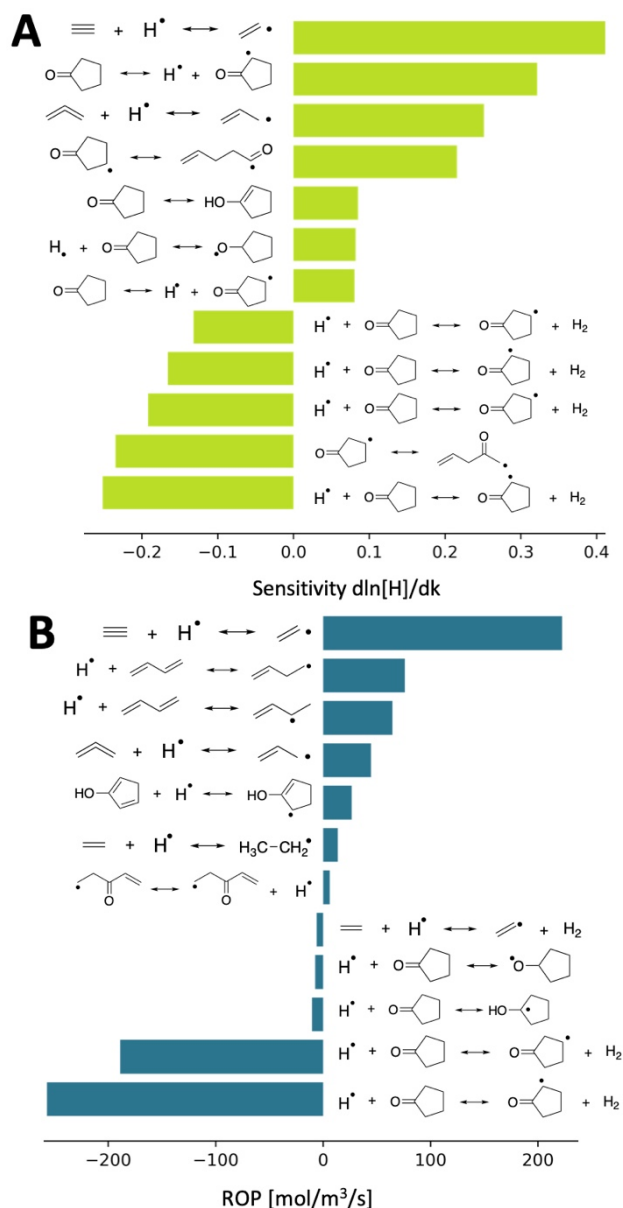
Figure 12. (A) Sensitivity and (B) ROP analysis (right) of H radical at 0.05 ms with the condition of $T_5 = 1393$ K, $P_5 = 8.977$ atm and $x_{CPO,0} = 4000$ ppm. The top 12 reactions (sorted by the absolute values) are shown for each analysis. The discrimination between the axial-H abstraction rates and the equatorial-H abstraction rates causes replications in the sensitivity analysis. Such discrimination is not maintained in the ROP analysis.

4.3.2 Transition stage

Due to the diminishing CPO concentration and the accumulation of C_2H_4 and other products (e.g., ketene), the secondary reactions between H radicals and products become comparable to the H abstraction of cyclopentanone. These reactions add additional consumption channels of H radical and thus cause a decrease in x_H, introducing the decomposition into the transition stage. When comparing the ROP results of H radicals at the beginning (Fig. 13(a)) and at the end of the transition stage (Fig. 13(b)), shifts can be seen from H radicals being dominantly consumed by cyclopentanone to H radicals being consumed by products. Moreover, some channels used to generate H radicals (like 3-buten-1-yl decomposing to

butadiene and H) in the early stage switch to H consumption during the transition stage. $x_{C_2H_4}/x_{CO}$ is less variant in the transition stage, mainly because of the increasing effect from the change in the primary reaction branching ratio (Fig. 10; more CPO proceeds via the unimolecular pathway) offsetting the impact from radical-product reactions becoming dominant. CPO is gradually consumed until the end of the stage when it is depleted. As consumption channels involving CPO no longer exist, and x_H reaches its local minimum and begins to increase.

4.3.3   Product pyrolysis stage

After the transition stage, as CPO is wholly consumed, the dominant species at this stage become the products, majorly consisting of ethylene and carbon monoxide as well as methane, ketene, allene, acetylene, and butadiene. Therefore, pyrolysis of the small hydrocarbon mixtures becomes dominant, which has been well studied in previous work [38–41]. Further, soot formation happens in this stage, as the formation of benzene and other species can be observed (a typical flux diagram can be found in the supplementary information Fig. S5.1).

5   Conclusions

In this work, we studied the pyrolysis of cyclopentanone (CPO) and presented a detailed kinetic model verified by shock tube and laser-absorption experiments. We measured the absorbance time-histories of CPO, C_2H_4, and CO simultaneously over a wide range of conditions and used $\alpha_{C_2H_4}/\alpha_{CO}$ time-history as one of the key factors to validate the models. To the best of our knowledge, we measured the first time-histories of these species during cyclopentanone pyrolysis over the temperature range of 1156-1416 K and pressure range of 8.53-10.06 atm. Additionally, we generated a comprehensive kinetic model using the Reaction Mechanism Generator (RMG) with refined parameters from literature and quantum calculations. The current model shows good agreement with the experimental time-histories. According to the ROP and sensitivity analysis, the model suggests that radical-involved pathways play essential roles in the cyclopentanone decomposition. During the early stage, when H radicals are accumulating, the radical-involved decomposition pathways are activated and become as crucial as pathway (1) and (2), resulting in $x_{C_2H_4}/x_{CO}$ decreasing swiftly. During the transition stage, reactions involving radicals and products become as important as reactions involving radicals and CPO due to the product accumulation, resulting in a decreasing x_H. During the product pyrolysis stage, the decomposition of the mixture of C_2H_4 and other products dominated as CPO is depleted. Our finding in this study contributes to the understanding of pyrolysis of cyclopentanone and establishes a more comprehensive combustion/pyrolysis model. Such understanding can also be helpful when proposing pyrolysis or combustion models for other biofuels.
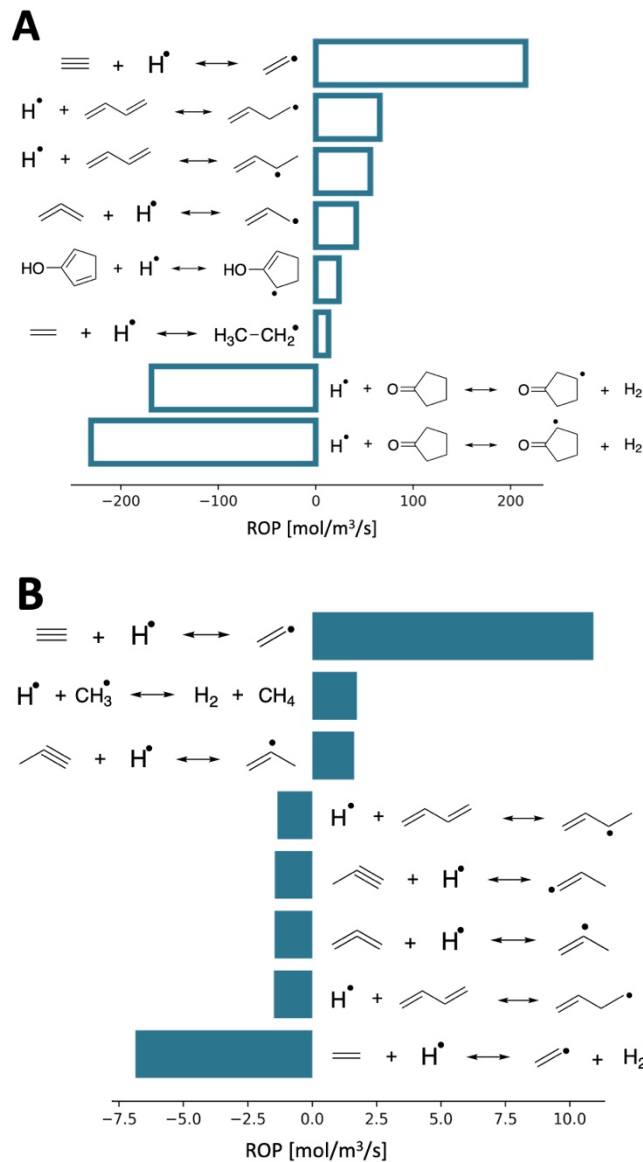
Figure 13. ROP analysis at $T_5 = 1393$ K, $P_5 = 8.977$ atm and $x_{CPO,0} = 4000$ ppm. (A) ROP of H radical at $t = t_1$ (0.1 ms, x_H reaching local maximum) (B) ROP of H radical at $t = t_2$ (1.76 ms, x_H reaching local minimum). The top 8 reactions are shown.

Acknowledgements

Disclaimer

This report was prepared as an account of work sponsored by an agency of the United States Government. Neither the United States Government nor any agency thereof, nor any of their employees, makes any warranty, express or implied, or assumes any legal liability or responsibility for the accuracy, completeness, or usefulness of any information, apparatus, product, or process disclosed, or represents that its use would not infringe privately owned rights. Reference herein to any specific commercial product, process, or

service by trade name, trademark, manufacturer, or otherwise does not necessarily constitute or imply its endorsement, recommendation, or favoring by the United States Government or any agency thereof. The views and opinions of authors expressed herein do not necessarily state or reflect those of the United States Government or any agency thereof.

Supplementary material

Supplementary material associated with this article can be found, in the online version, at [TBD]. The supplementary material includes the experimental setup information, *Ab Initio* Calculation details, detailed mechanism of cyclopentanone pyrolysis in CHEMKIN format, validation of the mechanism versus experiments, and the derivations of the uncertainty analysis.

References

[1] J. Farrell, Co-optimization of Fuels and Engines, National Renewable Energy Lab.(NREL), Golden, CO (United States), 2016.

[2] G.A. Strobel, B. Knighton, K. Kluck, Y. Ren, T. Livinghouse, M. Griffin, D. Spakowicz, J. Sears, The production of myco-diesel hydrocarbons and their derivatives by the endophytic fungus Gliocladium roseum (NRRL 50072), Microbiology. 154 (2008) 3319–3328.

[3] M.-H. Kao, R. Kumar Venkatraman, M.N. R. Ashfold, A. J. Orr-Ewing, Effects of ring-strain on the ultrafast photochemistry of cyclic ketones, Chem. Sci. (2020). https://doi.org/10.1039/C9SC05208A.

[4] K. Zhang, N. Lokachari, E. Ninnemann, S. Khanniche, W.H. Green, H.J. Curran, S.S. Vasu, W.J. Pitz, An experimental, theoretical, and modeling study of the ignition behavior of cyclopentanone, Proc. Combust. Inst. 37 (2019) 657–665.

[5] S. Thion, C. Togbé, G. Dayma, Z. Serinyel, P. Dagaut, Experimental and Detailed Kinetic Modeling Study of Cyclopentanone Oxidation in a Jet-Stirred Reactor at 1 and 10 atm, Energy Fuels. 31 (2017) 2144–2155.

[6] D. Gaspar, Top Ten Blendstocks for Turbocharged Gasoline Engines: Bio-blendstocks with the Potential to Deliver the Highest Engine Efficiency, Pacific Northwest National Laboratory, PNNL-28713, 2019.

[7] E.R. Johnson, W.D. Walters, The Thermal Decomposition of Cyclopentanone, J. Am. Chem. Soc. 76 (1954) 6266–6271.

[8] F.M. Delles, L.T. Dodd, L.F. Lowden, F.J. Romano, L.G. Daignault, The Pyrolysis of Cyclopentanone, J. Am. Chem. Soc. 91 (1969) 7645–7647.

[9] A.M. Zaras, S. Thion, P. Dagaut, Computational Kinetic Study for the Unimolecular Decomposition of Cyclopentanone, Int. J. Chem. Kinet. 47 (2015) 439–446.

[10] C.-W. Zhou, J.M. Simmie, W.J. Pitz, H.J. Curran, Toward the Development of a Fundamentally Based Chemical Model for Cyclopentanone: High-Pressure-Limit Rate Constants for H Atom Abstraction and Fuel Radical Decomposition, J. Phys. Chem. A. 120 (2016) 7037–7044.

[11] J.I.M. Pastoors, A. Bodi, P. Hemberger, J. Bouwman, Dissociative Ionization and Thermal Decomposition of Cyclopentanone, Chem. – Eur. J. 23 (2017) 13131–13140.

[12] E. Ninnemann, A. Laich, S. Neupane, S. Barak, S. Vasu, O. Pryor, Z. Loparo, Pyrolysis of cyclopentanone: A shock tube and laser absorption study, in: 2018 Jt. Propuls. Conf., American Institute of Aeronautics and Astronautics, Cincinnati, Ohio, 2018. https://arc.aiaa.org/doi/10.2514/6.2018-4474 (accessed September 4, 2019).

[13] B.R. Giri, M. AlAbbad, J.R. Barker, A. Farooq, High temperature unimolecular decomposition of cyclopentanone, Proc. Combust. Inst. 37 (2019) 267–273.

[14] A.G. Baboul, L.A. Curtiss, P.C. Redfern, K. Raghavachari, Gaussian-3 theory using density functional geometries and zero-point energies, J. Chem. Phys. 110 (1999) 7650–7657. https://doi.org/10.1063/1.478676.

[15] L.A. Curtiss, K. Raghavachari, P.C. Redfern, V. Rassolov, J.A. Pople, Gaussian-3 (G3) theory for molecules containing first and second-row atoms, J. Chem. Phys. 109 (1998) 7764–7776. https://doi.org/10.1063/1.477422.

[16] J.R. Barker, T.L. Nguyen, J.F. Stanton, C. Aieta, M. Ceotto, F. Gabas, T.J.D. Kumar, C.G.L. Li, L.L. Lohr, A. Maranzana, N.F. Ortiz, J.M. Preses, J.M. Simmie, J.A. Sonk, P.J. Stimac, MultiWell-2019 Software Suite, University of Michigan, Ann Arbor, Michigan, USA, 2019. http://clasp-research.engin.umich.edu/multiwell/.

[17] J.R. Barker, Multiple-Well, multiple-path unimolecular reaction systems. I. MultiWell computer program suite, Int. J. Chem. Kinet. 33 (2001) 232–245. https://doi.org/10.1002/kin.1017.

[18] J.R. Barker, Energy transfer in master equation simulations: A new approach, Int. J. Chem. Kinet. 41 (2009) 748–763. https://doi.org/10.1002/kin.20447.

[19] E. Ninnemann, B. Koroglu, O. Pryor, S. Barak, L. Nash, Z. Loparo, J. Sosa, K. Ahmed, S. Vasu, New insights into the shock tube ignition of H2/O2 at low to moderate temperatures using high-speed end-wall imaging, Combust. Flame. 187 (2018) 11–21. https://doi.org/10.1016/j.combustflame.2017.08.021.

[20] O. Pryor, S. Barak, B. Koroglu, E. Ninnemann, S.S. Vasu, Measurements and interpretation of shock tube ignition delay times in highly CO2 diluted mixtures using multiple diagnostics, Combust. Flame. 180 (2017) 63–76. https://doi.org/10.1016/j.combustflame.2017.02.020.

[21] B. Koroglu, S.S. Vasu, Measurements of Propanal Ignition Delay Times and Species Time Histories Using Shock Tube and Laser Absorption, Int. J. Chem. Kinet. 48 (2016) 679–690. https://doi.org/10.1002/kin.21024.

[22] K.A. Kobe, H.R. Crawford, R.W. Stephenson, Industrial Design Data—Critical Properties and Vapor Presesures of Some Ketones, Ind. Eng. Chem. 47 (1955) 1767–1772. https://doi.org/10.1021/ie50549a025.

[23] A. Barhala, D. Dragoescu, M. Teodorescu, I. Wichterle, Isothermal (vapour+liquid) equilibria in the binary mixtures (1,2-dichloroethane and 1,1,1-trichloroethane with cyclopentanone) within the temperature range (298.15 to 313.15)K, J. Chem. Thermodyn. 38 (2006) 617–623. https://doi.org/10.1016/j.jct.2005.07.016.

[24] W. Ren, D.F. Davidson, R.K. Hanson, IR laser absorption diagnostic for C2H4 in shock tube kinetics studies, Int. J. Chem. Kinet. 44 (2012) 423–432. https://doi.org/10.1002/kin.20599.

[25] Z.E. Loparo, J.G. Lopez, S. Neupane, W.P. Partridge, K. Vodopyanov, S.S. Vasu, Fuel-rich n-heptane oxidation: A shock tube and laser absorption study, Combust. Flame. 185 (2017) 220–233. https://doi.org/10.1016/j.combustflame.2017.07.016.

[26] M.J. Frisch, G.W. Trucks, H.B. Schlegel, G.E. Scuseria, M.A. Robb, J.R. Cheeseman, J.A. Montgomery Jr., T. Vreven, K.N. Kudin, J.C. Burant, J.M. Millam, S.S. Iyengar, J. Tomasi, V. Barone, B. Mennucci, M. Cossi, G. Scalmani, N. Rega, G.A. Petersson, H. Nakatsuji, M. Hada, M. Ehara, K. Toyota, R. Fukuda, J. Hasegawa, M. Ishida, T. Nakajima, Y. Honda, O. Kitao, H. Nakai, M. Klene, X. Li, J.E. Knox, H.P. Hratchian, J.B. Cross, V. Bakken, C. Adamo, J. Jaramillo, R. Gomperts, R.E. Stratmann, O. Yazyev, A.J. Austin, R. Cammi, C. Pomelli, J.W. Ochterski, P.Y. Ayala, K. Morokuma, G.A. Voth, P. Salvador, J.J. Dannenberg, V.G. Zakrzewski, S. Dapprich, A.D. Daniels, M.C. Strain, O. Farkas, D.K. Malick, A.D. Rabuck, K. Raghavachari, J.B. Foresman, J.V. Ortiz, Q. Cui, A.G. Baboul, S. Clifford, J. Cioslowski, B.B. Stefanov, G. Liu, A. Liashenko, P. Piskorz, I. Komaromi, R.L. Martin, D.J. Fox, T. Keith, M.A. Al-Laham, C.Y. Peng, A. Nanayakkara, M. Challacombe, P.M.W. Gill, B. Johnson, W. Chen, M.W. Wong, C. Gonzalez, J.A. Pople, Gaussian 03, Revision D.01, n.d.

[27] M.J. Frisch, G.W. Trucks, H.B. Schlegel, G.E. Scuseria, M.A. Robb, J.R. Cheeseman, G. Scalmani, V. Barone, G.A. Petersson, H. Nakatsuji, X. Li, M. Caricato, A.V. Marenich, J. Bloino, B.G. Janesko, R. Gomperts, B. Mennucci, H.P. Hratchian, J.V. Ortiz, A.F. Izmaylov, J.L. Sonnenberg, D. Williams-Young, F. Ding, F. Lipparini, F. Egidi, J. Goings, B. Peng, A. Petrone, T. Henderson, D. Ranasinghe, V.G. Zakrzewski, J. Gao, N. Rega, G. Zheng, W. Liang, M. Hada, M. Ehara, K. Toyota, R. Fukuda, J. Hasegawa, M. Ishida, T. Nakajima, Y. Honda, O. Kitao, H. Nakai, T. Vreven, K. Throssell, J.A. Montgomery Jr., J.E. Peralta, F. Ogliaro, M.J. Bearpark, J.J. Heyd, E.N. Brothers, K.N. Kudin, V.N. Staroverov, T.A. Keith, R. Kobayashi, J. Normand, K. Raghavachari, A.P. Rendell, J.C. Burant, S.S. Iyengar, J. Tomasi, M. Cossi, J.M. Millam, M. Klene, C. Adamo, R. Cammi, J.W. Ochterski, R.L. Martin, K. Morokuma, O. Farkas, J.B. Foresman, D.J. Fox, Gaussian 16, Revision B.01, 2016.

[28] C.W. Gao, J.W. Allen, W.H. Green, R.H. West, Reaction Mechanism Generator: Automatic construction of chemical kinetic mechanisms, Comput. Phys. Commun. 203 (2016) 212–225. https://doi.org/10.1016/j.cpc.2016.02.013.

[29] Reaction Mechanism Generator, https://github.com/ReactionMechanismGenerator/RMG-Py, Cambridge, Massachusetts, USA, 2019. https://github.com/ReactionMechanismGenerator/RMG-Py.

[30] CHEMKIN-PRO 15112, Reaction Design, San Diego, 2011.

[31] Reaction Mechanism Simulator, https://github.com/ReactionMechanismGenerator/ReactionMechanismSimulator.jl, 2019. https://github.com/ReactionMechanismGenerator/ReactionMechanismSimulator.jl.

[32] J.A. Montgomery, M.J. Frisch, J.W. Ochterski, G.A. Petersson, A complete basis set model chemistry. VI. Use of density functional geometries and frequencies, J. Chem. Phys. 110 (1999) 2822–2827. https://doi.org/10.1063/1.477924.

[33] J.G. Hill, K.A. Peterson, G. Knizia, H.-J. Werner, Extrapolating MP2 and CCSD explicitly correlated correlation energies to the complete basis set limit with first and second row correlation consistent basis sets, J. Chem. Phys. 131 (2009) 194105. https://doi.org/10.1063/1.3265857.

[34] A. Austin, G.A. Petersson, M.J. Frisch, F.J. Dobek, G. Scalmani, K. Throssell, A Density Functional with Spherical Atom Dispersion Terms, J. Chem. Theory Comput. 8 (2012) 4989–5007. https://doi.org/10.1021/ct300778e.

[35] H.-J. Werner, P.J. Knowles, G. Knizia, F.R. Manby, M. Schütz, Molpro: a general-purpose quantum chemistry program package, WIREs Comput Mol Sci. 2 (2012) 242–253.

[36] H.-J. Werner, P.J. Knowles, G. Knizia, F.R. Manby, M. Schütz, P. Celani, W. Györffy, D. Kats, T. Korona, R. Lindh, A. Mitrushenkov, G. Rauhut, K.R. Shamasundar, T.B. Adler, R.D. Amos, S.J. Bennie, A. Bernhardsson, A. Berning, D.L. Cooper, M.J.O. Deegan, A.J. Dobbyn, F. Eckert, E. Goll, C. Hampel, A. Hesselmann, G. Hetzer, T. Hrenar, G. Jansen, C. Köppl, S.J.R. Lee, Y. Liu, A.W. Lloyd, Q. Ma, R.A. Mata, A.J. May, S.J. McNicholas, W. Meyer, T.F.M. III, M.E. Mura, A. Nicklass, D.P. O'Neill, P. Palmieri, D. Peng, K. Pflüger, R. Pitzer, M. Reiher, T. Shiozaki, H. Stoll, A.J. Stone, R. Tarroni, T. Thorsteinsson, M. Wang, M. Welborn, MOLPRO, version 2019.2, a package of ab initio programs, molpro, 2019.

[37] N. Cohen, S.W. Benson, Estimation of heats of formation of organic compounds by additivity methods, Chem. Rev. 93 (1993) 2419–2438. https://doi.org/10.1021/cr00023a005.

[38] K. Norinaga, V.M. Janardhanan, O. Deutschmann, Detailed chemical kinetic modeling of pyrolysis of ethylene, acetylene, and propylene at 1073–1373 K with a plug-flow reactor model, Int. J. Chem. Kinet. 40 (2008) 199–208.

[39] M.P. Ruiz, A. Callejas, A. Millera, M.U. Alzueta, R. Bilbao, Soot formation from C2H2 and C2H4 pyrolysis at different temperatures, J. Anal. Appl. Pyrolysis. 79 (2007) 244–251. https://doi.org/10.1016/j.jaap.2006.10.012.

[40] T.-C. Chu, Z. J. Buras, P. Oßwald, M. Liu, M. Jacob Goldman, W. H. Green, Modeling of aromatics formation in fuel-rich methane oxy-combustion with an automatically generated pressure-dependent mechanism, Phys. Chem. Chem. Phys. 21 (2019) 813–832. https://doi.org/10.1039/C8CP06097E.

[41] D.M. Matheu, A.M. Dean, J.M. Grenda, W.H. Green, Mechanism Generation with Integrated Pressure Dependence: A New Model for Methane Pyrolysis, J. Phys. Chem. A. 107 (2003) 8552–8565. https://doi.org/10.1021/jp0345957.